Design and Synthesis of BAW Bandpass Filter Based on Inline NRN and Dangling Resonator Topology

Chiek Xin YOON [1], Socheatra SOEUNG [1], Sovuthy CHEAB [2], Peng Wen WONG [3], Chuan Ching Dennis LING [1]

[1] Dept. of Electrical and Electronic, Universiti Teknologi PETRONAS, Bandar Seri Iskandar, Perak 32610, Malaysia
[2] Cambodia Academy of Digital Technology, Phnom Penh, Cambodia
[3] FILPAL (M) Sdn Bhd, Bayan Lepas, Penang 11900, Malaysia

chiek_21000388@utp.edu.my, socheatra.s@utp.edu.my, sovuthy.cheab@cadt.edu.kh, peng@filpal.com, dennis.ling@utp.edu.my

Submitted April 30, 2024 / Accepted June 25, 2024 / Online first July 31, 2024

Abstract. *In this paper, a novel inline network realization of non-resonating node (NRN) and dangling resonator (R) pair direct synthesis approach is presented. Arbitrary prescribed transmission zeros at real frequencies are realized through independently controlling the dangling resonators of the NRN-R pairs with impedance inverters between adjacent nodes. The bandpass element values for fourth order acoustic wave filter with a center frequency at 98 MHz are obtained through execution and mapping of the synthesis results based on the Generalized Chebyshev polynomials. The layout of prototype is presented. Finally, the prototype is constructed and measured using network analyzer to validate the proposed concept in realizing the BAW filter using Butterworth Lowpass Van Dyke (BVD) model. The filter has an insertion loss of 3.45 dB, a return loss of 8.5 dB, and two transmission zeros (TZs). In terms of implementation, this synthesis technique allows flexibility to synthesize and realize a conventional filter with transmission zeros as an inline network without cross couplings. This offers advantages in terms of size and cost reduction in filter production due to the inline resonator arrangement and reduced sensitivity in the design and tuning process.*

Keywords

BAW bandpass filter, dangling resonator, direct synthesis approach, inline, non-resonating node

1. Introduction

With the growth of wireless applications and occupied bandwidth for data transfer and communication between mobile devices, filters are employed to properly isolate the required bandwidth to avoid crosstalk and reject unwanted noise signals. In wireless and mobile communications systems, a filter must achieve a remarkable performance [1]. High quality factor (Q), low insertion loss (IL), high return loss (RL), sharp transition slopes and high out-of-band rejection are the characteristics of high performance of a bandpass filter [2]. Compact size, high power handling and selectivity, low weight and loss microwave filter is demanding specifically in cellular communications base-stations [3] whereas the increasing market demands for high performance and miniature acoustic wave filter is stimulated by the compact and multi-band mobile application. Theoretically, at certain frequencies, the wavelength and propagation velocity of electromagnetic waves are directly related to the device size. Consequently, acoustic waves result in smaller device sizes due to their propagation velocity being approximately four to five times slower than that of electromagnetic waves [4]. There are two types of bulk acoustic wave (BAW) resonators used in telecommunication systems, Film Bulk Acoustic Resonator (FBAR) and Solidly Mounted Resonator (SMR). A computation method of BAW filters is presented in [5] which involves comparing the equivalent impedance of Butterworth Van Dyke (BVD) model with the impedance calculated using one-dimensional piezoelectric equations for a piezoelectric structure. BVD models are very useful, prompting researchers to modify the BVD model to account for analysis of significant differences in electrode thickness of FBAR filters [6]. Analysis of spurious effects at the series resonance of BAW filters due to the resistance of thin metallic electrodes could be conducted by modifying the Mason and BVD models, as presented in [7]. With its geometric conditions, the design of BAW filter requires a ladder type of topology. In recent years, new conceptual designs and syntheses concerning the filter configurations were studied and reported [8–18]. The syntheses of extracted-pole configurations reported in [8–12], although they allow for inline topologies, are not easy to design and are not suitable to realize the BAW resonators. More effective ways to realize the inline topology are by using frequency-dependent coupling which require special coupling resonators or structures suitable for cavity or planar structures [13–17]. The conventional design synthesis of microwave filters with finite transmission zeros is achieved by introducing cross-coupled configuration which requires complex realization, and it is not suitable in BAW filter designs. An alternative method shows in-line topology is feasible by introducing non-resonating node [18].

DOI: 10.13164/re.2024.0477

In this paper, a novel synthesis approach for the inline filter network with NRN-R pairs is introduced and presented. A filter network which has derived eigenvalues and couplings can be represented by an admittance function with transversal array. The transversal array is reconfigured as an inline NRN-R pair acoustic wave ladder network by introducing a phase shifter to the input. To illustrate the synthesis, the design example of the 4th order bandpass filter is synthesized and fabricated using Lowpass BVD model. Finally, the lowpass to bandpass BVD model is applied to achieve the desired bandpass filter.

2. Synthesis of Inline NRN-R Network

Generally, a filter network can be represented by an admittance function with transversal array as shown in Fig. 1 where the eigenvalues and couplings are derived. The reconfiguration of eigenvalues or couplings is feasible by introducing a phase shifter at the input or output ports without distorting the filter response. A phase shifter can be modelled by the transfer matrix as shown below

$$\mathbf{T}_1 = \begin{bmatrix} -\dfrac{\cot(\varphi_1)}{\csc(\varphi_1)} & -\dfrac{\mathrm{j}}{\csc(\varphi_1)} \\ -\mathrm{j}\csc(\varphi_1) + \dfrac{\mathrm{j}\cot(\varphi_1)^2}{\csc(\varphi_1)} & -\dfrac{\cot(\varphi_1)}{\csc(\varphi_1)} \end{bmatrix}. \quad (1)$$

With the introduction of a phase shifter at the input port and applying two port parameter conversion, the equivalent admittance function parameters of a filter network are obtained:

$$y'_{11\mathrm{n}} = \cos(\varphi_1) y_{11\mathrm{n}} + \mathrm{j}\sin(\varphi_1) y_{\mathrm{d}}, \quad (2)$$

$$y'_{\mathrm{d}} = \cos(\varphi_1) y_{\mathrm{d}} + \mathrm{j}\sin(\varphi_1) y_{11\mathrm{n}}, \quad (3)$$

$$y'_{21\mathrm{n}} = -y_{21\mathrm{n}}, \quad (4)$$

$$y'_{22\mathrm{n}} = \cos(\varphi_1) y_{22\mathrm{n}} y_{\mathrm{d}} + \mathrm{j}\sin(\varphi_1) y_{11\mathrm{n}} y_{22\mathrm{n}} - \mathrm{j}\sin(\varphi_1) y_{21\mathrm{n}}^2 \quad (5)$$

where y_{d} and $y_{ij\mathrm{n}}$ are the denominator and numerator of the respective admittance function parameters. To extract a transmission zero or NRN-R pair, the admittance matrix is evaluated at a position of transmission zero at a real frequency and by solving (3). The phase φ_1 can be easily determined as

$$\varphi_1 = \mathrm{j}\tan^{-1}\left(\frac{y_{\mathrm{d}}}{y_{11\mathrm{n}}}\right)\Bigg|_{s=\mathrm{j}\omega_{\mathrm{z1}}} \quad (6)$$

where s is the complex frequency and ω_{z1} is the transmission zero. Having determined the phase φ_1 from the prescribed transmission zero and substituting into (2)–(5), it can be noticed that a new set of eigenvalues and couplings is achieved. One of its eigenvalues is now equal to the value of the desired transmission zero.

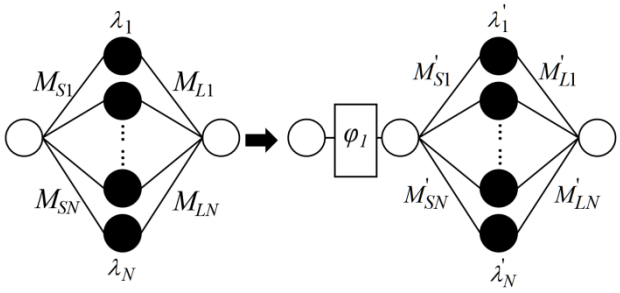

Fig. 1. Equivalence transversal array network with configured eigenvalues.

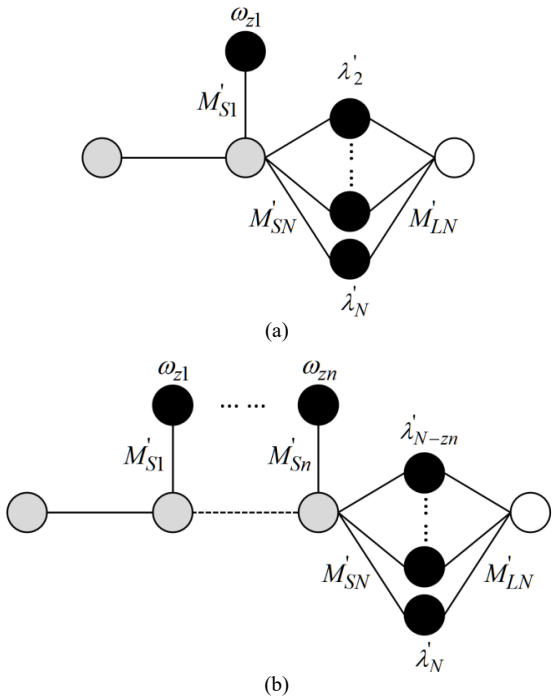

Fig. 2. (a) Transversal array with extracted NRN-R pair. (b) Transversal array with extracted NRN-R pair.

It is also interesting to note that coupling M_{Li} of eigenvalue λ_i is diminished to zero resulting in a new transversal array network with a dangled resonator at the input of the network as shown in Fig. 2(a). The residues of the new admittance functions can be deduced by

$$r'_{21_i} = \left.\frac{y'_{21\mathrm{n}}}{\dfrac{\partial\left(y'_{\mathrm{d}}\right)}{\partial s}}\right|_{s=\mathrm{j}\lambda'_i}, \quad (7)$$

$$r'_{11_i} = \left.\frac{y'_{11\mathrm{n}}}{\dfrac{\partial\left(y'_{\mathrm{d}}\right)}{\partial s}}\right|_{s=\mathrm{j}\lambda'_i}, \quad (8)$$

$$r_{22_i}^{'} = \left.\frac{y_{22\mathrm{n}}^{'}}{\frac{\partial\left(y_{\mathrm{d}}^{'}\right)}{\partial s}}\right|_{s=\mathrm{j}\lambda_i^{'}} \tag{9}$$

where the port susceptance y_{b1} can now be obtained by letting s approaching infinity

$$y_{b1} = \lim_{s\to\infty}\left(\frac{y_{11\mathrm{n}}^{'}}{y_{\mathrm{d}}^{'}}\right). \tag{10}$$

The same process can be repeated for the extraction of NRN-R pairs from the remaining network. The nth order inline NRN-R pairs coupling matrix is shown in (11).

$$\begin{bmatrix} \cot\varphi_i & -\csc\varphi_i & 0 & 0 \\ -\csc\varphi_i & \cot\varphi_i + \cot\varphi_{i+1} - \mathrm{j}y_{b,i} & \ddots & 0 \\ 0 & \ddots & \ddots & -\csc\varphi_n \\ 0 & 0 & -\csc\varphi_n & \cot\varphi_n - \mathrm{j}y_{b,n} \end{bmatrix} \tag{11}$$

2.1 Illustration of Coupling Matrix Synthesis

Consider a fourth-order inline filter with $N = 4$, ω_i = [–3,–3,+3,+3] is synthesized with NRN pair where N is filter order and ω_i is the position of transmission zeros. The filter topology of 4th order acoustic wave ladder network and its coupling matrix representation are shown in Fig. 3 and (12).

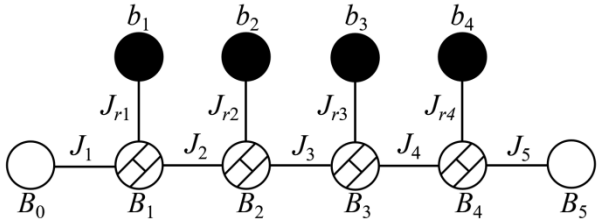

Fig. 3. Filter topology of 4th order acoustic wave ladder network.

$$\begin{bmatrix} B_0 & J_1 & 0 & 0 & 0 & 0 & 0 & 0 & 0 & 0 \\ J_1 & B_1 & J_{r1} & J_2 & 0 & 0 & 0 & 0 & 0 & 0 \\ 0 & J_{r1} & b_1 & 0 & 0 & 0 & 0 & 0 & 0 & 0 \\ 0 & J_2 & 0 & B_2 & J_{r2} & J_3 & 0 & 0 & 0 & 0 \\ 0 & 0 & 0 & J_{r2} & b_2 & 0 & 0 & 0 & 0 & 0 \\ 0 & 0 & 0 & J_3 & 0 & B_3 & J_{r3} & J_4 & 0 & 0 \\ 0 & 0 & 0 & 0 & 0 & J_{r3} & b_3 & 0 & 0 & 0 \\ 0 & 0 & 0 & 0 & 0 & J_4 & 0 & B_4 & J_{r4} & J_5 \\ 0 & 0 & 0 & 0 & 0 & 0 & 0 & J_{r4} & b_4 & 0 \\ 0 & 0 & 0 & 0 & 0 & 0 & 0 & J_5 & 0 & B_5 \end{bmatrix} \tag{12}$$

where

$$\begin{cases} b_i = \omega_i \\ J_i = -\csc(\varphi_i) \\ J_{ri} = \sqrt{r_{11i}}\big|_{s=\mathrm{j}\lambda_i} \\ B_0 = \cot(\varphi_1) \\ B_5 = \cot(\varphi_4) \\ B_i = \cot(\varphi_i) + \cot(\varphi_{i+1}) - \mathrm{j}y_{b,i} \\ J_5 = 1 \end{cases} \quad ,i = 1,2,...,N \tag{13}$$

With the desired design specification, generalized Chebyshev filtering function can be used to synthesize the filter. $F(s)$, $P(s)$ and $E(s)$ polynomials are obtained using recursive technique respectively as:

$$F(s) = s^4 + 1.029s^2 + 0.1403 + 0.1\mathrm{j}, \tag{14}$$

$$P(s) = s^4 + 18s^2 + 81, \tag{15}$$

$$E(s) = s^4 + 2.105s^3 - 2.10^{-15}\,\mathrm{j}s^3 + 3.249s^2 - 5.10^{-15}\,\mathrm{j}s^2 + 2.822s + 1.404 - 6.474^{-16}\,\mathrm{j}. \tag{16}$$

With this complex form of polynomials, the transmission and reflection coefficients S_{21} and S_{11} can be obtained:

$$S_{21} = \frac{P(s)}{\varepsilon E(s)}, \tag{17}$$

$$S_{11} = \frac{F(s)}{\varepsilon_{\mathrm{R}} E(s)}. \tag{18}$$

Figure 4 shows the ideal fourth-order generalized Chebyshev lowpass filter responses with 4 poles in the passband and 2 pairs of transmission zeros at –3 and 3.

Applying the synthesis in Sec. 2, the coupling matrix is deduced as shown in (19).

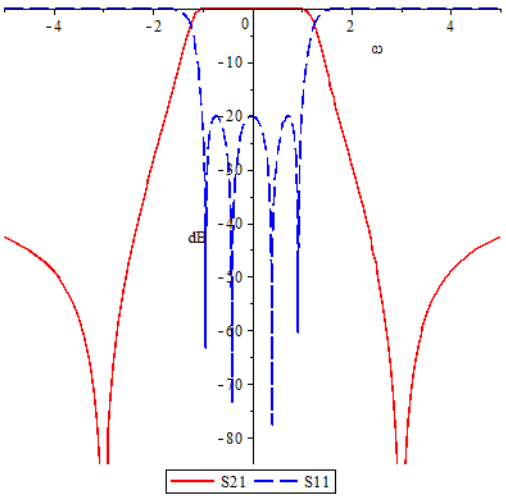

Fig. 4. 4th order ideal lowpass filter transfer and reflection characteristics.

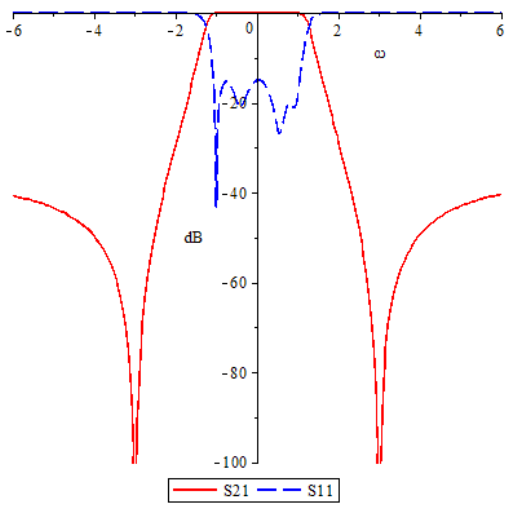

Fig. 5. Transfer and reflection characteristics based on synthesized coupling matrix.

$$\begin{bmatrix}
-0.3867 & 1.072 & 0 & 0 & 0 & 0 & 0 & 0 & 0 & 0 \\
1.072 & -2.708 & 2.708 & -1.034 & 0 & 0 & 0 & 0 & 0 & 0 \\
0 & 2.708 & -3 & 0 & 0 & 0 & 0 & 0 & 0 & 0 \\
0 & -1.034 & 0 & 3.827 & 3.310 & 1.023 & 0 & 0 & 0 & 0 \\
0 & 0 & 0 & 3.310 & 3 & 0 & 0 & 0 & 0 & 0 \\
0 & 0 & 0 & 1.023 & 0 & -4.318 & 3.516 & -1.095 & 0 & 0 \\
0 & 0 & 0 & 0 & 0 & 3.516 & -3 & 0 & 0 & 0 \\
0 & 0 & 0 & 0 & 0 & -1.095 & 0 & 2.689 & 2.698 & 1 \\
0 & 0 & 0 & 0 & 0 & 0 & 0 & 2.698 & 3 & 0 \\
0 & 0 & 0 & 0 & 0 & 0 & 0 & 1 & 0 & 0.4458
\end{bmatrix} \tag{19}$$

Figure 5 shows the transfer and reflection characteristics of the filter based on the synthesized coupling matrix.

2.2 Butterworth Lowpass Van Dyke (BVD) Model Formulation

The use of NRN in filtering structure was introduced by Amari [19] which demonstrated that this utilization may reduce the size of filter in particular cases. A dangling resonator is a structure formed by three components which are NRN, resonating node (RN) and coupling where the node symbols are shown in Fig. 6. NRN implemented with an FIR B internally connected to ground and an admittance inverter J_r that represents the coupling between the former nodes whereas RN is formed by a unit capacitor in parallel with a frequency-independent reactance b. The input admittance of a dangling resonator is

$$Y_{\text{in}}(s) = \text{j}B + \frac{J_r^2}{s + \text{j}b}. \tag{20}$$

When $s = -\text{j}b$, the input admittance becomes infinite, that is at the position of TZ at normalized frequency $\omega = -b$. Alternatively, an attenuation zero is produced when the input admittance is zero. The signal is directed to propagate

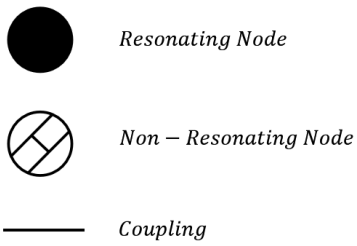

Fig. 6. Nodes symbols of the dangling resonator.

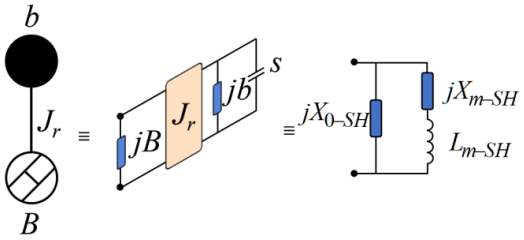

Fig. 7. Equivalence between the dangling structure and the circuital representation of a BVD resonator in lowpass for shunt resonator [12].

from source to load through the NRN. The admittance characteristics observed in dangling resonators resemble those found in lowpass normalized frequency BVD model.

Butterworth Van Dyke (BVD) model is developed by Giménez [11]. It is generally acknowledged that the Butterworth Van Dyke (BVD) electrical model, which consists of a series LC resonator in the motional arm in parallel with the static capacitance reflecting the electrical characteristics of piezoelectric resonators in the main resonance frequency.

Figure 7 shows the equivalence between the dangling structure and the circuital representation of a BVD resonator in lowpass for series resonator. By analyzing the input admittance expression of dangling resonator and lowpass BVD circuits, resulting the relationship between shunt dangling resonator and lowpass BVD:

$$L_{m-SH} = \frac{1}{J_r^2}, \tag{21}$$

$$X_{m-SH} = \frac{b}{J_r^2}, \tag{22}$$

$$X_{0-SH} = -\frac{1}{B}. \tag{23}$$

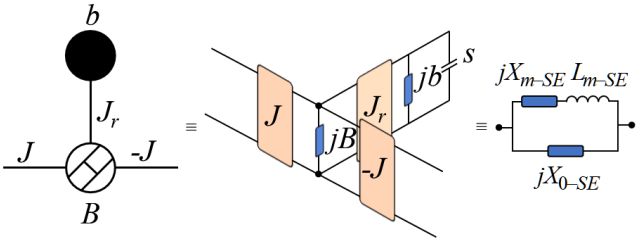

Fig. 8. Equivalence between the dangling structure and the circuital representation of a BVD resonator in lowpass for series resonator [20].

Figure 8 shows the equivalence between the dangling structure and the circuital representation of a BVD resonator in lowpass for series resonator. On the other hand, the relationship between series dangling resonator and lowpass BVD:

$$L_{m-SE} = \frac{B^2}{J_r^2 J^2}, \tag{24}$$

$$X_{m-SE} = \frac{B}{J^2}\left(\frac{bB}{J_r^2} - 1\right), \tag{25}$$

$$X_{0-SE} = -\frac{B}{J_r^2}. \tag{26}$$

3. Bandpass Filter Network Transformation

Having mapped the coupling matrix to BVD model resonators, the equivalent lowpass network can be formed. To realize the bandpass filter network, the BVD bandpass transformation is required. Figure 9 shows the equivalence between the lowpass and bandpass BVD model of an acoustic wave resonator. The bandpass BVD model consists of series resonator composed of L_a and C_a representing the acoustic path of acoustic wave resonator, and the static capacitance C_0 corresponding to IDT of SAW resonator or parallel electrode plates of BAW resonator. On the other hand, the lowpass BVD model consists of X_0 and X_m, frequency invariant reactance and L_m, lowpass inductor.

Bandpass domain is achieved by a proper frequency transformation from lowpass BVD model. The input impedances of the lowpass and bandpass BVD model are obtained:

$$Z_{\text{in}}(\Omega) = \frac{\mathrm{j}X_0(\Omega L_m + X_m)}{\Omega L_m + X_m + X_0}, \tag{27}$$

$$Z_{\text{in}}(\omega) = \frac{\mathrm{j}\left(\omega L_a - \dfrac{1}{\omega C_a}\right)}{1 - \omega^2 C_0 L_a + C_0 / C_a}. \tag{28}$$

To achieve the bandpass BVD model elements, firstly, the lowpass impedance is converted to bandpass impedance using the following transformation.

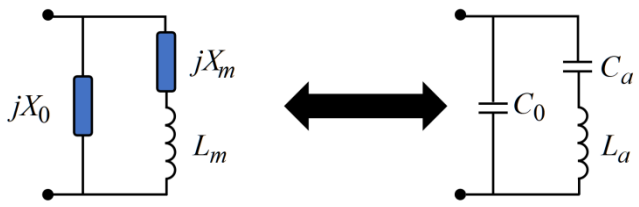

Fig. 9. Lowpass and bandpass BVD equivalent model of an acoustic wave resonator [20].

$$\Omega = \alpha\left(\frac{\omega}{\omega_0} - \frac{\omega_0}{\omega}\right) \tag{29}$$

where α is the bandwidth scaling factor, ω is the bandpass frequency variable, and ω_0 is the geometric midband frequency:

$$\omega_0 = \sqrt{\omega_1 \omega_2}\,. \tag{30}$$

ω_1 and ω_2 are the lower and upper edge frequencies of the desired bandpass frequency. By substituting (29) into (27), a new bandpass impedance expression can be obtained. Comparing and solving both transformed bandpass impedance and bandpass BVD impedance models at ω_0, the bandpass circuit elements at the center frequency ω_0 can be defined as

$$L_a = \frac{Z_0}{2}\left(\frac{2\alpha L_m + X_m}{\omega_0}\right), \tag{31}$$

$$C_a = \frac{2}{Z_0}\frac{1}{\omega_0(2\alpha L_m - X_m)}, \tag{32}$$

$$C_0 = -\frac{1}{Z_0}\frac{1}{\omega_0 X_0}. \tag{33}$$

4. Bandpass Filter Prototype Realization

From coupling synthesis, we extract the elements of 4th order acoustic wave filter as tabulated in Tab. 1. With the extracted elements, the nodal representation of a 4th order ladder network can be constructed starting from a series resonator as presented in Fig. 10.

i	J_i	J_{ri}	B_i	b
0	-	-	–0.3867	-
1	1.0722	2.7076	–2.7081	–3
2	–1.0344	3.3100	3.82699	3
3	1.0239	3.51588	4.31797	–3
4	–1.09487	2.69796	2.68885	3
5	–0.38673	-	0.445824	0

Tab. 1. Extracted elements of 4th order acoustic wave filter.

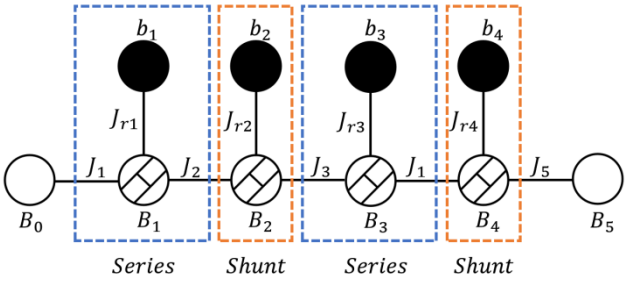

Fig. 10. Nodal representation of a 4th order acoustic wave ladder network starting in series resonator.

i	L_{mi}	X_{mi}	X_{0i}
1	0.9020	–0.2642	–2.442
2	0.09128	0.2738	–0.2613
3	1.345	–0.1846	–3.852
4	0.1374	0.4121	–0.3719

Tab. 2. Lowpass BVD circuits elements of 4th order acoustic wave filter.

i	L_{ai}	C_{ai}	C_{0i}
1	3.481×10^{-7}	7.209×10^{-12}	1.337×10^{-11}
2	4.749×10^{-8}	1.060×10^{-10}	1.250×10^{-10}
3	5.278×10^{-7}	4.910×10^{-12}	8.477×10^{-12}
4	7.148×10^{-8}	7.043×10^{-11}	8.779×10^{-11}

Tab. 3. Bandpass elements of 4th order acoustic wave filter.

The lowpass BVD circuits elements are determined from (21) to (26) for series and shunt resonators as shown in Tab. 2.

To proceed for bandpass transformation, the lowpass BVD circuit is transformed to a bandpass filter with the lower- and upper-cutoff frequency at $f_1 = 88$ MHz and $f_2 = 108$ MHz. From (29)–(33), the bandpass elements are determined and obtained as shown in Tab. 3.

The bandpass filter circuit is constructed in advanced design system (ADS) and simulated to observe the transfer and reflection characteristics where the results are shown in Fig. 12.

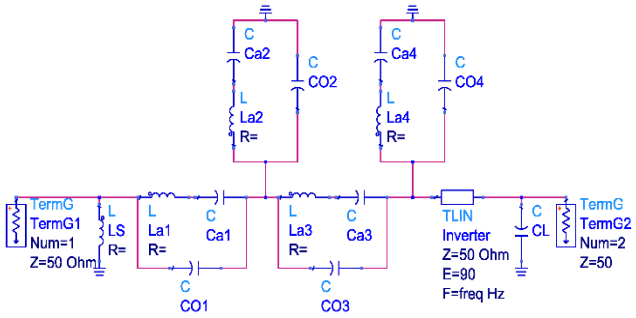

Fig. 11. An equivalent BVD bandpass filter circuit.

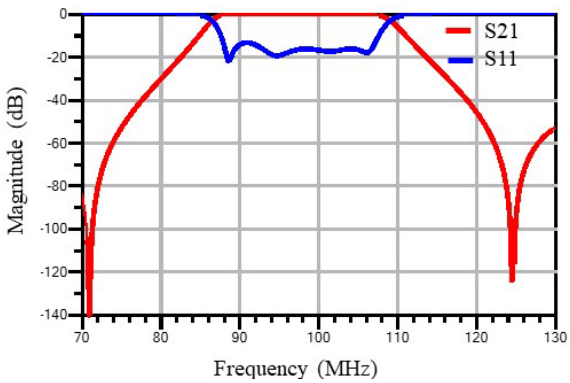

Fig. 12. Simulated S11 and S21 responses based on BVD model.

Having obtained the desired filter responses, the next step is to generate the layout. First, it starts by checking the components available in the market and modeling those components, including their parasitic parameters, at the circuit simulation level. After that, the layout can be generated from the circuit. To ensure that the layout and selected circuit components produce the desired responses, ADS co-simulation is required. This involves using internal ports in ADS momentum to generate the *n*-port Touchstone file and importing it into the circuit simulation with the selected components. If the simulated results still meet the specifications, the next stage is to send the layout for fabrication. Otherwise, fine-tuning of the layout and component parameters needs to be redone.

5. Experimental Results and Discussions

The layout was designed using ADS momentum. The layout then was exported and fabricated on FR4 board with dielectric thickness of 1.5 mm, the dielectric constant of 4.9, loss tangent of 0.08, and copper thickness of 35 µm. Due to the unavailability of the exact bandpass element values in Tab. 3, off-the-shelf elements of the closest values are purchased in prototyping the 4th order acoustic wave filter as shown in Fig. 13. The performance of 4th order acoustic wave filter prototype is measured in the laboratory using Keysight Network Analyzer (PNA E8363C). Figure 14 illustrates the measured and simulated results of the bandpass filter. The prototype has a bandwidth of 15 MHz with a return loss of 8.5 dB and the insertion loss of 3.45 dB compared to the simulated network with a bandwidth of 20 MHz, the return loss of 7.48 dB and the insertion loss of 0.7 dB.

The poor filter performance and shifts in frequencies and discrepancies between the prototype and the simulated network responses are due to parasitic parameters (inductances and capacitances), fringing capacitance, and the low-quality factor of the components on the board. Additionally, the values of the purchased components are not the same as those of the simulated components. This is due to the non-availability of exact component values in the market and component tolerances. These frequency-dependent parameters have caused shifts in frequencies and reduced bandwidth. Combined with the lossy characteristics of the RF4

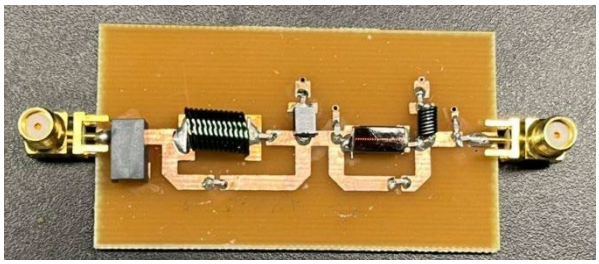

Fig. 13. 4th order acoustic wave filter prototype with off-the-shelf resonators.

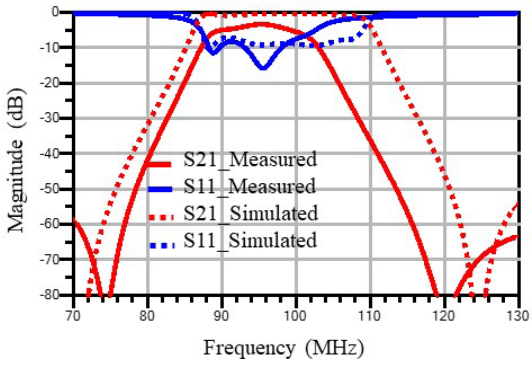

Fig. 14. Transfer and reflection characteristics of the prototype and simulated network.

Ref	Topology	Selectivity
[15]	Inline resonators with direct couplings	Symmetric and asymmetric with N-1 TZs
[13]	Inline main line resonator couplings	Symmetric and asymmetric with number of TZ based on the shortest path
[11]	Inline structure broken into the designs of a cascade of elementary blocks	Symmetric and asymmetric with several TZs based on properly selecting blocks
[14]	Inline cascading square open-loop resonators	Chebyshev type
[12]	Inline structure without NRN or a phase shifter	Chebyshev type with a pair of TZs
This work	Inline NRN and dangling resonator	Symmetric and asymmetric generalized Chebyshev type with independently controlled dangling resonators

Tab. 5. The state-of-the-art comparison of filter performances.

board, this has a significant impact on the filter performance, leading to a lossy performance, rounding off of the pass-band, and shifts in the lower and upper frequencies. The state-of-the-art comparison of filter syntheses and performances is depicted in Tab. 5.

6. Conclusion

This paper presents a novel synthesis technique of an inline dangling resonator pair for the realization of an acoustic wave filter circuit. With this synthesis technique, the flexibility to synthesize and realize a conventional filter with arbitrary transmission zeros as an inline network with inverters between adjacent nodes can be achieved. It provides the feasibility to realize a bandpass BAW filter based on BVD model mapping. The illustration of coupling matrices is shown with a 4^{th} order generalized Chebyshev filter example. The mapping and network transformation have been demonstrated to realize the 4^{th} order acoustic wave bandpass filter. The filter prototype was constructed on an FR4 board with a center frequency of 98 MHz, an insertion loss of 3.45 dB, a return loss of 8.5 dB, and two transmission zeros. The measurement results show good agreement with the design theory which is suitable in designing FBAR filters.

Acknowledgments

This work was supported by Universiti Teknologi PETRONAS and YUTP-PRG (015PBC-007) funding on this research.

References

[1] CHEAB, S., WONG, P. W. Design and synthesis of microwave dual mode filter. In *2012 IEEE Asia-Pacific Conference on Applied Electromagnetics (APACE)*. Melaka (Malaysia), 2012, p. 226–229. DOI: 10.1109/APACE.2012.6457665

[2] MAHON, S. The 5G effect on RF filter technologies. *IEEE Transactions on Semiconductor Manufacturing,* 2017, vol. 30, no. 4, p. 494–499. DOI: 10.1109/TSM.2017.2757879

[3] CHEAB, S., WONG, P. W. Design and synthesis of quasi dual-mode, elliptic coaxial filter. *Radioengineering*, 2015, vol. 24, no. 3, p. 795–799. DOI: 10.13164/re.2015.0795

[4] ASHRAF, N., MESBAH, Y., EMAD, A., et al. Enabling the 5G: Modelling and design of high Q film bulk acoustic wave resonator (FBAR) for high frequency applications. In *2020 IEEE International Symposium on Circuits and Systems (ISCAS)*. Seville (Spain), 2020, p. 1–4. DOI: 10.1109/ISCAS45731.2020.9180652

[5] AMARI, S., ROSENBERG, U. Synthesis and design of novel in-line filters with one or two real transmission zeros. *IEEE Transactions on Microwave Theory and Techniques*, 2014, vol. 52, no. 5, p. 1464–1478. DOI: 10.1109/TMTT.2004.827023

[6] FAN, J., CHATRAS, M., CROS, D. Synthesis method for BAW filters computation. In *IEEE International Conference on Electronics, Circuits and Systems.* Nice (France), 2006, p. 391–394, DOI: 10.1109/ICECS.2006.379807

[7] CHAO, M. C., HUANT, Z. N., PAO, S. Y., et al. Modified BVD-equivalent circuit of FBAR by taking electrodes into account. In *Proceedings of 2002 IEEE Ultrasonics Symposium*. Munich (Germany), 2002, vol. 1, p. 973–976. DOI: 10.1109/ULTSYM.2002.1193558

[8] LUGO-HERNÁNDEZ, E., COLLADO, C., MATEU, J., et al. Modified Mason's and BVD models for analysis of spurious modes due to ohmic losses in BAW resonators. In *2021 Joint Conference of the European Frequency and Time Forum and IEEE International Frequency Control Symposium (EFTF/IFCS)*. Gainesville (FL, USA), 2021, p. 1–3. DOI: 10.1109/EFTF/IFCS52194.2021.9604279

[9] MONTEJO-GARAI, J. R., RUIZ-CRUZ, J. A., REBOLLAR, J. M., et al. Synthesis and design of in-line N-order filters with N real transmission zeros by means of extracted poles implemented in low-cost rectangular H-plane waveguide. *IEEE Transactions on Microwave Theory and Techniques*, 2005, vol. 53, no. 5, p. 1636–1642. DOI: 10.1109/TMTT.2005.847053

[10] AMARI, S., MACCHIARELLA, G. Synthesis of inline filters with arbitrarily placed attenuation poles by using nonresonating nodes. *IEEE Transactions on Microwave Theory and Techniques*, 2005, vol. 53, no. 10, p. 3075–3081. DOI: 10.1109/TMTT.2005.855128

[11] MACCHIARELLA, G., TAMIAZZO, S. An application-oriented design procedure for cascaded-block extracted-pole filters. *IEEE Transactions on Microwave Theory and Techniques*, 2021, vol. 69, no. 1, p. 647–658. DOI: 10.1109/TMTT.2020.3035367

[12] YANG, Y., ZENG, Y., YU, M., et al. Synthesis of a new class of extracted pole filters without the ideal phase shifters. *IEEE Transactions on Microwave Theory and Techniques*, 2021, vol. 69, no. 1, p. 639–646. DOI: 10.1109/TMTT.2020.3038398

[13] TAMIAZZO, S., MACCHIARELLA, G., SEYFERT, F. Path filters: A class of true inline topologies with transmission zeros. *IEEE Transactions on Microwave Theory and Techniques*, 2022,

vol. 70, no. 1, p. 850–863. DOI: 10.1109/TMTT.2021.3126861

[14] NWAJANA, A. O., OBI, E. R. Application of compact folded-arms square open-loop resonator to bandpass filter design. *Micromachines*, 2023, vol. 14, no. 2, p. 1–10. DOI: 10.3390/mi14020320

[15] HE, Y., MACCHIARELLA, G., MA, Z., et al. Advanced direct synthesis approach for high selectivity in-line topology filters comprising N–1 adjacent frequency-variant couplings. *IEEE Access*, 2019, vol. 7, p. 41659–41668. DOI: 10.1109/ACCESS.2019.2907531

[16] MACCHIARELLA, G., BASTIOLI, S., SNYDER, R. V. Design of in-line filters with transmission zeros using strongly coupled resonators pairs. *IEEE Transactions on Microwave Theory and Techniques*, 2018, vol. 66, no. 8, p. 3836–3846. DOI: 10.1109/TMTT.2018.2840981

[17] AMARI, S., ROSENBERG, U., BORNEMANN, J. Singlets, cascaded singlets, and the nonresonating node model for advanced modular design of elliptic filters. *IEEE Microwave and Wireless Components Letters*, 2004, vol. 14, no. 5, p. 237–239. DOI: 10.1109/LMWC.2004.827866

[18] WONG, P. W., NG, G. S. A new class of inline microwave filter with transmission zeros. In *IEEE/MTT-S International Microwave Symposium (IMS 2023)*. San Diego (CA, USA), 2023, p. 740–743. DOI: 10.1109/IMS37964.2023.10188050

[19] GIMÉNEZ, A., VERDÚ, J., DE PACO SÁNCHEZ, P. General synthesis methodology for the design of acoustic wave ladder filters and duplexers. *IEEE Access*, 2018, vol. 6, p. 47969–47979. DOI: 10.1109/ACCESS.2018.2865808

[20] TRIANO NOTARIO, Á. Advanced synthesis techniques for parallel-connected and cross-coupled filters based on acoustic wave technologies. *Ph.D. Dissertation*. Autonomous University of Barcelona, 2020, p. 1–181.

About the Authors …

Chiek Xin YOON received her bachelor's degree in Electrical and Electronic Engineering from Universiti Teknologi PETRONAS, Perak, Malaysia in 2019. She is currently pursuing her M.Sc. in Electrical and Electronics Engineering at UTP. Her research interest includes inline network realization with direct synthesis approach.

Socheatra SOEUNG (corresponding author, Senior Member, IEEE) received his B.Eng. (Honors) degree in Electrical and Electronics, major in Computer System Architecture from Universiti Teknologi PETRONAS, Malaysia. He completed his M.Sc. and Ph.D. degrees by research in RF and microwave engineering from Universiti Teknologi PETRONAS, Malaysia. He was awarded and funded as a research officer in RF microwave engineering under several Ministry of Higher Education Malaysia and industrial funding projects during his graduate study. He was involved in designing, implementing, and testing RF subsystem components and RF communication link. Currently, he works as a lecturer and a computation and communication cluster leader in Universiti Teknologi PETRONAS in Electrical and Electronics Engineering department. He has been awarded with more than 10 fundings from Malaysian Gov't, industries, and University research collaborations. Over the years, he has been a contributor to more than 35 technical research journal and conference papers. His research interests include RF microwave filter design and synthesis for multiband, multi-mode filter on planar and cavity structures, computer-aided tuning and optimization techniques. He is currently an IEEE, MTT member, Associate Fellow of the ASEAN Academy of Engineering and Technology, and serves as a secretary of IEEE ED/MTT/SSC Penang Chapter, Malaysia.

Sovuthy CHEAB (Senior Member, IEEE) earned his Ph.D., Master of Science, and Bachelor of Engineering in Electrical and Electronics Engineering majoring in Communication Systems (Telecommunication) from Universiti Teknologi PETRONAS (UTP), Malaysia in 2016, 2012, and 2011, respectively. He has experience in teaching and conducting research in the field of telecommunications for over 10 years and has published more than 50 technical research papers. He supervised a total of 6 Ph.D. and 7 master students. He served as an Executive Committee Member of the IEEE ED/MTT/SSC Penang Chapter, from 2016 to 2023, and had been elected as the secretary of the Chapter for 2021 to 2022 term. His research interest is in RF & microwave engineering and also Internet of Things. After completing his Ph.D., he was a faculty member of Electrical and Electronic Engineering Department at UTP for a period of 6 years from 2016 to 2021. He then worked as Technical Director in FILPAL (M) Sdn Bhd for one year before returning to Cambodia in 2022 to work as Director of Makerspace and Senior Researcher at Cambodia Academy of Digital Technology (CADT). Starting from 2024, he has been appointed as Dean of School of Digital Engineering in CADT. He is a Senior Member of IEEE, Associate Fellow of the ASEAN Academy of Engineering and Technology, and Steering Committee of ASEAN IVO, a global alliance of ICT R&D institutes and universities in the ASEAN region and Japan.

Peng Wen WONG was born in Perak, Malaysia, in 1984. He received the B.Eng. (Hons. First-Class) degree and Ph.D. in Microwave Engineering from the University of Leeds, United Kingdom. He then joined Intel Malaysia and worked as a Test R&D engineer. He received research funding from the Ministry of Defense, UK where he completed his Ph.D. in the University of Leeds in 2009. During the Ph.D. degree, he was involved in a U.K. DTI-funded project, developing process design kits for multilayer system-in-package modules. He worked as an Associate Professor with the Petronas University of Technology, Perak, Malaysia from 2010 to 2019. From 2019–2021, he was with Huawei Sweden and worked as Principal Engineer and Program Manager, leading 5G research team for the development of next generation 5G massive MIMO base station. He received 2019 Future Star Award and Individual Performance Award 2020 from Huawei Sweden. Currently he is the CEO of FILPAL SDN BHD, driving RF Design & Manufacturing businesses and the development of RF supply chain ecosystem. Recently he is awarded SME ICONS RECOGNITION 2023 for the outstanding leadership and contribution to industry, community, and the Malaysian services sector. Dr. Wong is also an Associate Fellow of the AAET. He has served as an invited speaker locally and internationally including at APMC 2017 and a keynote speaker at ICCSP 2017. He is currently an Advisor of the IEEE Penang Joint Chapter. He has served as the

Technical Chair for IMESS 2017 and 2018. He was the Former Chair of the IEEE ED/MTT/SSC Penang Chapter, from 2016 to 2017. He was the Founding Chair of the IEEE International Microwave, Electron Devices, and Solid-State Symposium (IMESS), in 2016. He serves as a Reviewer for the IEEE Transactions on Microwave Theory and Techniques, the IEEE Microwave and Wireless Components Letters, IET Microwaves, Antennas and Propagation.

Chuan Ching Dennis LING embarked on a professional career as a Mathematics Lecturer in Universiti Teknologi PETRONAS. Over the 12 years, he has gained recognition for his work in mathematical modelling, nonlinear fluid mechanics and seismic wave analysis. Dennis's innovative approach and dedication to mathematical modelling with analysis have made a significant impact in forecasting failure in monitoring system. Throughout his career, Dennis has achieved several milestones, including inhouse and international projects. His work in fluid mechanics and wave responses has been particularly influential, earning him respect and admiration from peers and industry leaders alike.